International Journal on Recent and Innovation Trends in Computing and Communication
ISSN: 2321-8169 Volume: 11 Issue: 10
Article Received: *25 July 2023* ***Revised:*** *14 September 2023* ***Accepted:*** *28 September 2023*

"Enhancing Power System Stability with Fuzzy-PI Cascade Controllers and TCSC: A Comprehensive Study"

Nimmakanti Anil[1*], Dr.G.Balaji[2]

[1*]Research scholar, Faculty of Engineering and Technology, Annamalai University, Chidambaram, Tamil Nadu 608002, aniljitseee@gmail.com
[2]Associate Professor, Faculty of Engineering and Technology, Annamalai University, Chidambaram, Tamil Nadu 608002, balaji.g.au@gmail.com

***Corresponding Author:** Nimmakanti Anil
*Research scholar, Faculty of Engineering and Technology, Annamalai University, Chidambaram, Tamil Nadu 608002, aniljitseee@gmail.com

ABSTRACT

This study endeavours to develop cascade controllers employing Fuzzy-PI methodology to enhance power system stability, with a specific focus on generation control. The primary goal is to mitigate system instabilities and improve the reliability and performance of contemporary power grids. The efficacy of the Fuzzy-PI controller is assessed through extensive simulations involving significant fluctuations in wind energy generation, with comparative analysis against traditional PI controllers. Furthermore, the research emphasizes fortifying the stability of modern power systems by deploying optimized controllers, specifically targeting challenges related to frequency and voltage stability through the application of tailored controllers for Thyristor Controlled Series Capacitor (TCSC). The overarching objectives include enhancing both frequency and voltage stability through the utilization of TCSC units. Moreover, the research integrates hybrid optimization techniques, such as Improved meta-heuristic MPR-RSA, to fine-tune controller parameters, ensuring optimal performance across diverse operating conditions. The selection of controller gains relies on the integral absolute time error function, serving as the cost function for problem optimization.

Keywords: **-** Power system stability, Thyristor Controlled Series Capacitor (TCSC), Frequency stability, Voltage stability, Generation control, Fuzzy-PI controller, Improved meta-heuristic MPR-RSA.

INTRODUCTION

The long-term viability of power systems is crucial to ensuring the dependable and efficient operation of electrical grids. The demand for sophisticated control strategies grows as renewable energy sources are integrated more and more into contemporary power networks, which increases their complexity. One promising avenue for enhancing power system stability involves the integration of fuzzy logic and proportional-integral-derivative (PI) controllers in a cascade configuration. [1] This approach leverages the strengths of both fuzzy logic, which can handle complex and uncertain systems, and PI controllers, known for their simplicity and effectiveness. The combination of Fuzzy-PI cascade controllers offers a robust and adaptive solution to address the dynamic and nonlinear nature of power systems. Fuzzy logic enables the incorporation of human-like reasoning and linguistic rules, allowing the controller to make decisions based on imprecise and uncertain information. This is particularly advantageous in power systems, where factors such as varying load demands, renewable energy intermittency, and unforeseen disturbances contribute to system complexity. The Fuzzy-PI cascade structure allows for a hierarchical control framework, where the fuzzy controller provides high-level decision-making, and the PI controller refines the output based on the system's error.

This research aims to investigate the synergies between Fuzzy-PI cascade controllers in enhancing power system stability. The research will examine the controllers' design and tuning, taking into account the particulars of the power system in question [3], [2]. Through comprehensive simulation studies and real-world applications, the effectiveness of the proposed approach will be evaluated, offering valuable insights into its potential for practical implementation in power systems. As the power industry continues to evolve, with an increasing focus on sustainability and grid resilience, the development of advanced control strategies becomes crucial. This research on Fuzzy-PI cascade controllers contributes to the ongoing efforts in creating robust and adaptive solutions for power system stability, addressing the challenges posed by the changing landscape of energy generation and consumption. The results of this study could influence future developments in power system control & aid in the creation of intelligent and durable electrical grids.

Power System Stability

Power system stability is a fundamental and critical aspect of electrical engineering that ensures the reliable and secure

International Journal on Recent and Innovation Trends in Computing and Communication
ISSN: 2321-8169 Volume: 11 Issue: 10
Article Received: *25 July 2023* ***Revised:*** *14 September 2023* ***Accepted:*** *28 September 2023*

operation of interconnected power networks. [4] In this sense, stability refers to the power system's capacity to continue operating synchronously in the wake of disruptions such abrupt changes in load or breakdowns. The dynamic nature of power systems, influenced by factors like changing demand, renewable energy integration, and unexpected disturbances, makes stability a challenging yet essential consideration. Transient stability & steady-state stability are the two main categories of power system stability. [5], [15] The ability of the network to retain synchronism and recover following a disruption, such as a fault or abrupt shift in load, is known as transient stability. Steady-state stability, on the other hand, focuses on the ability of the system to reach a new equilibrium and maintain it under varying operating conditions. [6] Both forms of stability are crucial for preventing cascading failures and ensuring the continuous and secure supply of electrical power to consumers.

Various factors impact power system stability, including the inertia of generators, the strength of the transmission network, and the control mechanisms in place. Enhancing power system stability is largely dependent on modern control strategies and technology proportional-integral-derivative (PI) and fuzzy logic controllers. [7] Ongoing research and technological advancements continue to refine and improve methods for assessing, monitoring, and enhancing power system stability, contributing to the overall reliability and resilience of electrical grids worldwide [8].

Contribution:

The main of the study is to Enhancing Power System Stability with Fuzzy-PI Cascade Controllers in this study hybrid Improved meta-heuristic MPR-RSA. For cluster head selection and rooting scheme.

Organization:

In this study we organize firstly related work taken by the topic and secondly we have taken background from the topic and thirdly write about methodoly and results part and finally conclusion.

RELATED WORK

[9] Super-capacitor and redox flow battery hybrid energy storage devices are also added to report more and study system dynamics. A sensitivity investigation shows that the increased QOAOA proposed controller, estimated under limited conditions, can adapt to significant system changes. In conclusion, a real-time hardware-in-the-loop (HIL) simulation using OPAL-RT shows that the smart grid AGC challenge controller is viable.

[10] It looks at the best low-frequency oscillation solution for power systems. In order to create an intelligent controller, the study combines a power system stabilizer. This study examines three PSS design approaches: fractional-order proportional-integral-derivative (FPI), lead-lag (LL), and proportional-derivative-integral (PI). Power oscillation dampers are not as effective as the FOPI -based PSS, as demonstrated by the static VAR compensator (SVC). [11] To establish a performance benchmark, the EOA-FOPI controller—a fixed-coefficient variation based on the optima FOPI controller—was created. In multi-machine interconnected power systems, static synchronous series compensators (SSSCs) are used and contrasted with other well-liked control techniques. The comparisons show how successfully settling time, overshoot, while undershoot are improved, and system fluctuations are decreased using the EOA-AFFOPI control method.

[12] An intelligent control approach was proposed to improve the frequency dynamic efficiency of linked multi-source power systems that include gas, hydro, thermal power plants, and high wind energy penetration. In abnormal conditions, the restrictions of a proportional-integral-derivative (PI) controller are overcome by using fuzzy logic control and a PI controller. Furthermore, the Fuzzy-PI controller is improved by the recently implemented arithmetic optimisation algorithm (AOA), which overcomes the drawbacks of heuristic and traditional optimisation techniques. [13] First-time use of satin bower bird optimizer maximizes secondary controller gains. Comparing the results to other current controllers shows the recommended controller's superiority. It is also examined how RES and EV generation affects cascaded FOID-FOPD controller dynamics. Additionally, a sensitivity analysis shows that the cascaded FOID-FOPD controller's optimal gains can tolerate capacity ratio, disco participation matrix, load perturbations, and RESs.

[14] In two-area multisource hybrid power systems, automated load frequency control (ALFC) was investigated. In order to equilibrium system generation and demand, the HPS model incorporates both traditional and renewable energy sources. The Hankel model order reduction technique was utilised to investigate the robustness of the nonlinear dynamic HPS model. An effort was made to use cascade (PI-PD) control to manage HPS. By using PSO-GSA to minimize the integral absolute error (IAE) of the area control error, the gains of the controller were maximized.

A. Improved meta-heuristic MPR-RSA

BACKGROUND

One optimization technique for locating the best answer in an area of search is RSA. Since the RSA operates in a gradient-free fashion, it can quickly detect and resolve the problem. The drawback of traditional RSA is that it hinders search efficiency during the exploration stage because of local optimum challenges. This paper offers a newly developed MPR-RSA technique that generally yields the best results possible in order to address this problem. Reptiles are regarded by RSA as crocodiles when conducting searches.

Initialization of agents

The RSA method performs local as well as global searches in search space by using the social, surrounding, and hunting behaviours of crocodiles. The P-number population serves as the algorithm's starting point. To optimize, consider the

International Journal on Recent and Innovation Trends in Computing and Communication
ISSN: 2321-8169 Volume: 11 Issue: 10
Article Received: *25 July 2023* ***Revised:*** *14 September 2023* ***Accepted:*** *28 September 2023*

number of crocodiles, dimension size (d), and number of possible solutions (N).

Exploration (encircling phase)

Crocodiles exhibit two types of movement in their encircling mechanism: both high and belly walking. The crocodile's motions prevent it from discovering the greatest meal in the search space, unlike the secondary search. Consequently, the RSA algorithm's hunting behaviour may be carried out more easily with the use of the high and belly walking mechanism. By dividing the iteration into four techniques, four criteria can be used to achieve this condition. The best answer is identified during the investigation phase by utilizing the first two procedures. The plan for belly walking is predicated on i $< 2\frac{I}{4}$ and i $> \frac{I}{4}$, Although the high walking approach is implemented using the standards of i $\leq \frac{I}{4}$. Therefore, Eqs. (1) and (2) provide the updated position for finding the prey throughout the encircling phase.

$$S_{(x,y)}(i+1) = A_y(i) \times -\delta_{(x,y)}(i) \times \lambda - B_{(x,y)}(i) \times rn \quad (1)$$

Here, i $\leq \frac{I}{4}$.

$$S_{(x,y)}(i+1) = A_y(i) \times -S_{(n_1,y)}(i) \times es(i) \times rn \quad (2)$$

Here, i $< 2\frac{I}{4}$ and i $> \frac{I}{4}$.

Here, $A_y(i)$ gives the optimal solution at yth place, i, where I represents the maximum and current iteration values. Subsequently, λ denotes the variable that is sensitive to regulate the high walking strategy's correctness during its iterations, which is set to be 0.1, and r n is the random that lies in the range of 0 and 1. The word refers $S_{(n_1,y)}$ to the solution's random position, and n1 gives an arbitrary value b/w 1 and *N*, where *N* is the average number of candidate solutions. The term $\delta_{(x,y)}$ shows the yth position hunting parameter in the xth solution, as defined by Eq. (3), and $B_{(x,y)}$ is the search space's reduction function, which is obtained in

$$\delta_{(x,y)} = A_y(i) \times D_{(x,y)} \quad (3)$$

$$B_{(x,y)} = \frac{A_y(i) - s_{(n_2,y)}}{A_y(i) + \sigma} \quad (4)$$

Here, n_2 gives a random integer between 1 and N, where the smalls values is represented by σ.

The local optimum in the RSA method is being eluded in the first iteration with the help of exploitation behaviour. Consequently, this study presents the MPR-RSA algorithm, which addresses this problem by changing the sensitive parameters, λ and ω, to modify the evolutionary sense of RSA, which is what the probability ratio represents. According to these criteria, the local optima become stagnant during the course of the iterations during both the circling and hunting phases. Therefore, Eq. (5) provides the mathematical term for the MPR-RSA algorithm.

$$esi = 2 \times n_3 \times \left[1 - \left(\frac{i/I}{\lambda - \omega}\right)\right] \quad (5)$$

The adapted sense es(i) is defined by using Eq. (5), which yields a likelihood ratio that can be chosen arbitrarily and minimizes values within 2 and − 2 over the number of iterations. In a natural sense, the distribution of values is used to regulate the number of iterations and the pace of convergence throughout the population's activation of the given algorithm, es(i). In this case, there are 25 iterations total. The correlation value, denoted by "2" in the equation above, n3's value falls among -1 and 1, ranging from 2 to 0, and ω is the reactive parameter that, by estimating the disparity between solutions, provides the investigation precision for the hunting phase. This parameter should have fixed at 0.1. Equation (3), $D_{(x,y)}$, which is calculated using Eq. (6), between the current solution and the yth location of the ideal solution.

International Journal on Recent and Innovation Trends in Computing and Communication
ISSN: 2321-8169 Volume: 11 Issue: 10
Article Received: *25 July 2023* ***Revised:*** *14 September 2023* ***Accepted:*** *28 September 2023*

$$D_{(x,y)} = \omega + \frac{s_{(x,y)} - avg(s_x)}{A_y(i) \times (upper_y - lower_y) + \sigma}$$
$$\frac{d\delta}{dt} = \omega_b (\omega - 1) \quad (6)$$

The terms $upper_y$ and $lower_y$ indicate, respectively, the upper and lower limits of the yth position.. Then, $avg(s_x)$ yields the mean positions of the xth position as formulated in Eq. (7)

$$avg(s_x) = \frac{1}{N} \sum_{y=1}^{N} s_{(x,y)} \quad (7)$$

Exploitation (hunting phase)

Instead of encircling their prey, crocodiles can seek for nearly-optimal solutions for their position update by searching the target prey. The remaining two searching space tactics are put to use during the exploitation phase. The terms "hunting coordination" refer to the two tactics, which are dependent on i ≤ $3\frac{I}{4}$ and i > $2\frac{I}{4}$, where hunting collaboration is carried out between i ≤ I and i > $3\frac{I}{4}$. Thus, using Eqs. (8) and (9) Position update is determined for exploitation

.

$$s_{(x,y)}(i+1) = A_y(i) \times D_{(x,y)}(i) \times rn \quad (8)$$

Here, i ≤ $3\frac{I}{4}$ and i > $2\frac{I}{4}$.

$$s_{(x,y)}(i+1) = A_y(i) - \delta_{(x,y)}(i) \times \sigma - B_{(x,y)}(i) \times rn \quad (9)$$

When i ≤ I and i > $3\frac{I}{4}$, it is formulated .

Consequently, the discovery phase is completed when the need is met by i ≤ $\frac{I}{2}$ moreover, the exploitation stage has occurred when i > $\frac{I}{2}$. Ultimately, as Fig. 2 illustrates, the two stages of the suggested method can yield the best result by utilizing local optima and exploring space. Below is a description of the suggested MPR-RSA algorithm's pseudo-code.

Algorithm 1: Proposed MPR-RSA algorithm

```
Initialize P number of population
Initialize the parameters λ and ω
Initialize N the number of candidate solutions
Compute the probability ratio es
while (i < I) do
  Set the fitness function for solutions
  Find the accurate solution
  Using Eq. (5) es is computed
  For(x = 1 to N) do
    For(y = 1 to d) do
      Compute δ, B and D by using Eq. (3), Eq. (4), and Eq. (6), correspondingly
      If(i ≤ I/4) then
        Evaluate high walking by using Eq. (1)
      Else if (i ≤ 2I/4 and i > I/4) then
        Determine belly walking by Eq. (2)
      Else if (i ≤ 3I/4 and i > 2I/4) then
        Using Eq. (8), hunting coordination is estimated
      else
        Using Eq. (9), hunting cooperation is derived
      End if
    End for
  End for
  i = i + 1;
End while
Return the best solution
```

International Journal on Recent and Innovation Trends in Computing and Communication
ISSN: 2321-8169 Volume: 11 Issue: 10
Article Received: *25 July 2023* ***Revised:*** *14 September 2023* ***Accepted:*** *28 September 2023*

Weighted feature selection technique

Determining the weighted feature selection is prompted in order to increase the predicted accuracy. The suggested MPR-RSA technique uses the extracted features (F E f z) that have been gathered to determine the optimal solution for ambient air features . Feature selection has the benefit of delivering the most pertinent results for the needed model.

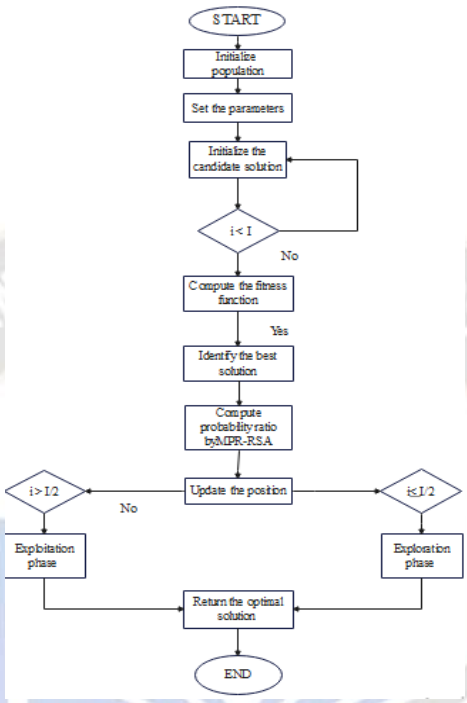

Figure 1 Flowchart representation of proposed MPR-RSA algorithm

METHODOLOGY

A. *Thyristor Controlled Series Compensation (TCSC)*

A (TCR) and a number of fixed capacitor banks are used in conjunction by TCSC controllers, as seen in Fig. 1. This combination introduces an inductive reactance to the line and allows for smooth adjustment of the capacitive response over a wide range. It can also be instructed to switch to a complete cycle state, in which the unidirectional Thyristor pairs conduct constantly.

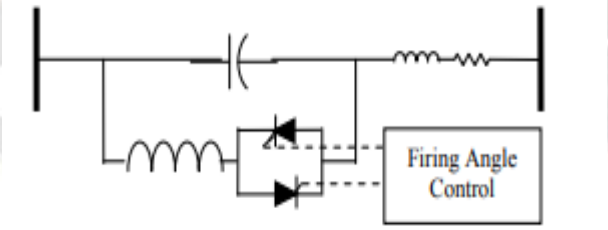

Figure 2 TCSC Layout configuration

II. POWER SYSTEM MODEL

The single machine limitless bus system in Fig. 2 featuring an TCSC at the end of the line is examined in this study. Appendix A contains the system data.

International Journal on Recent and Innovation Trends in Computing and Communication
ISSN: 2321-8169 Volume: 11 Issue: 10
Article Received: *25 July 2023* ***Revised:*** *14 September 2023* ***Accepted:*** *28 September 2023*

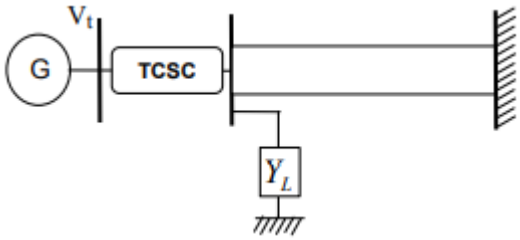

Figure 3 Single Machine Infinite Bus (SMIB) with TCSC

B. Generator Model

In this research, the generator is represented by a third-order model based on its internal voltage equations and electromechanical swing equation. This investigation examines IEEE Type-ST1 excitation. The following is the whole system model:

$$\frac{d\delta}{dt} = \omega_b(\omega - 1) \quad (1)$$

$$\frac{d\omega}{dt} = \frac{T_m - T_e - D(\omega - 1)}{M} \quad (2)$$

$$\frac{dE'q}{dt} = \frac{E_{fd} - (x_d - x'_d)i_d - E'_q}{T'_{do}} \quad (3)$$

$$\frac{dE_{fd}}{dt} = \frac{k_a(V_{ref} - V_t) - E_{fd}}{T_a} \quad (4)$$

$$T_e = v_q i_q + v_d i_d \quad (5)$$

Where,

- δ is the phase difference between E'_q and V_b
- E'_q is the internal voltage of the machine ?
- ω_b is the angular base speed .
- ω is the angular speed per unit .
- M is the machine inertia constant
- D is the damping coefficient
- Tm and Te are input and output torque of the generator respectively
- E_{fd} is the field voltage
- T_{do}' is the open-circuit field time constant ,
- x_d & x_d' are the d-axis reactance and d-axis transient reactance of the generator respectively.
- i_d & i_d' are the d-axis and q-axis transient current of the generator respectively .

TCSC Integration Analysis

Assess the effect of integrating the TCSC on the stability of the system's frequency, taking into account the control signal supplied by:

$$X_{TCSC}(t) = X_{nom} + K_{t\,csc}\Delta f(t) \quad (22)$$

Where:

X_{nom} is the nominal reactance of TCSC, $K_{t\,csc}$ is the TCSC control gain, $\Delta f(t)$ is the deviation in system frequency.

International Journal on Recent and Innovation Trends in Computing and Communication
ISSN: 2321-8169 Volume: 11 Issue: 10
Article Received: *25 July 2023* ***Revised:*** *14 September 2023* ***Accepted:*** *28 September 2023*

Basic principles and models of TCSC

In the TCSC module, an inductor, anti-parallel regulated Thyristor, and capacitor are connected in series and parallel. The variable resistor MOV & parallel bypass breaker CB prevent overvoltage & regulate any capacitor attached to the line. The fundamental idea behind TCSC is to produce a continuously regulated inductive & capacitive impedance by using a (TCR) to offset the capacitive reactance of multiple series capacitors.

By adjusting the thyristor's trigger angle α, the TCSC may modify the Thyristor branch current and, therefore, the TCSC branch's corresponding reactance value. The TCSC module's LC circuit's basic reactance is

$$\begin{aligned} X_{TCSC} &= K_\beta X_C \\ &= \left[1+\frac{\omega_0^2}{\pi(\omega_0^2-\omega^2)}\left(\frac{4\omega\cos^2\beta\tan\beta}{\omega_0+\omega}-2\beta-\sin\beta\right)\right] \\ &\times\left(-\frac{1}{\omega C}\right)=-\frac{1}{\omega C}-\frac{\omega_0^2}{\pi C(\omega_0^2-\omega^2)}\frac{4\cos^2\beta\tan\beta}{\omega_0+\omega} \\ &+\frac{(2\beta+\sin\beta)\omega_0^2}{\pi\omega C(\omega_0^2-\omega^2)} \end{aligned} \tag{23}$$

(1) XC represents capacitive impedance, ω represents basic angle frequency, Kβ represents TCSC reactance standard value, and ω0 represents resonant angle frequency. β is equal to π - α. The TCSC access system's corresponding power injection model is displayed in Figure 2.

The system's TCSC influence is projected onto and superimposed upon nodes i and j at the branch's termini. The TCSC is typically thought of as a series connection to a system with a variable reactance. The original network's node admittance matrix is symmetrical, even if the TCSC adds injection energy for virtual equivalent. The TCSC injects active and reactive power into system nodes I and J, which are,

$$P_i=\frac{U_iU_j}{X_{TCSC}}\sin(\delta_i-\delta_j) \tag{24}$$

$$Q_i=\frac{U_i}{X_{TCSC}}\left[U_i-U_j\cos(\delta_i-\delta_j)\right] \tag{25}$$

$$P_j=\frac{U_iU_j}{X_{TCSC}}\sin(\delta_j-\delta_i) \tag{26}$$

$$Q_j=\frac{U_j}{X_{TCSC}}\left[U_j-U_i\cos(\delta_j-\delta_i)\right] \tag{27}$$

where the voltages of the bus nodes i, j, are represented by Ui, Uj, and their corresponding voltage phases are represented by δi, δj.

From (1) to (5), the trigger angle is continually modified to vary the equivalent reactance of the TCSC, which optimises the power flow distribution and modifies the line's active and reactive power distribution. Figure 3 illustrates how the firing angle, or impedance, varies in response to the power passing through the line in order to modify the overall reactance of the TCSC. This compensates the line reactance and reduces power oscillation.

Fuzzy Logic Control System

The schematic representation of the enclosed-loop fuzzy control system is depicted in the fig. To accommodate the non-fuzzy variables with definite values, both the command and plant output undergo fuzzification. Before applying the fuzzy algorithm's fuzzy logic control to the controlled plant, it must be defuzzified because the plant cannot directly react to fuzzy logic controls. The components of a rule basis consist of doubtful rules, while the database includes membership functions corresponding to fuzzy subsets. Fuzzy rules can include fuzzy variables, membership functions, and conditional statements. The fuzzy control approach sequentially applies fuzzy rules using compositional inference & fuzzy implication rules. Fuzzy logic controllers are resilient, deterministic, non-linear model-free controllers.

International Journal on Recent and Innovation Trends in Computing and Communication
ISSN: 2321-8169 Volume: 11 Issue: 10
Article Received: *25 July 2023* ***Revised:*** *14 September 2023* ***Accepted:*** *28 September 2023*

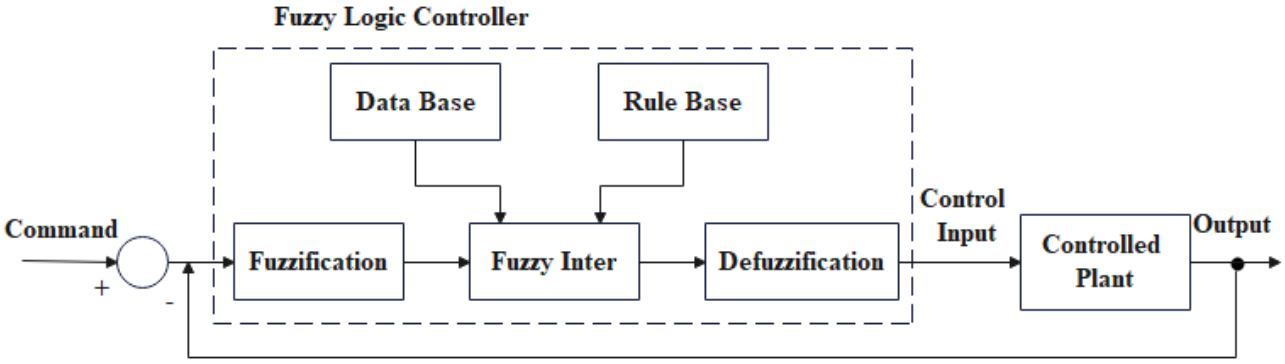

Fuzzy PI Control Rules

Imagine a fuzzy PI controller with two inputs along with a single output. FLC input fuzzy variables are e and change-of-error, and output fuzzy variable is incremental input. The discourse universes of *e*, e_c, and Δu are denoted by $E \subset R$ $\overline{E} \subset R$ and $U \subset R$, respectively. As shown before, fuzzy conditional statements are the common way that fuzzy principles are expressed.

$$R_i : IF\ e\ is\ A_i\ AND\ is\ B_i,\ THEN\ \Delta u\ is\ C_i \quad (18)$$

Fuzzy subsets inside the discourse world $E, \overline{E}\ and\ U$ are represented by the membership functions $\mu_{Ai}(e), \mu_{B_i}(e_c)$ and , respectively, denoted as A_i, B_i, and C_i. The fuzzy rule R_i able to conceptualised as a z-fuzzy relationship connecting the universes ($E, \overline{E}\ and\ U$). If each fuzzy variable *e*, e_c, or Δu has n fuzzy subsets, then the fuzzy rules total number is $I=n^2$. The set of ambiguous rules in question has the potential to be merged into a single rule using the union operator described below:

$$F = \frac{1}{\sum_{j=1}^{k}\left(w_1\left|e(j)\right| + w_2\left|e_c(j)\right|\right)}$$

$w_1\ and\ w_2$

$$u(k) = u(k-1) + g\Delta u^*(k) \qquad \Delta u = (e\ and\ e_c) \circ R \quad (20)$$

$a_e, b_e, a_{e_c}, a_{\Delta u}, f_{norm.e}, f_{norm.e_c}\ and\ g$

$e, e_c, \Delta u$

$$R = R_1 \cup R_2 \cup .....R_l \quad (19)$$

Once the max-min inference technique has been implemented, the output that follows is acquired. Nevertheless, this output number is still a fuzzy amount, therefore to turn it into a crisp value, one more step—the de-fuzzification process—is required. The most often used centre-of-gravity approach is favoured in order to get the obtaining precise value from the conclusions drawn from all relevant regulations. The centroid de-fuzzification method calculates the weighted average inside the function of membership curve of the ultimate fuzzy output to find the most common crisp answer for the fuzzy quantity. This method aims to identify a representative crisp value that captures the central tendency of the fuzzy set, offering a more concrete and easily interpretable output in applications where a single, well-defined value is desirable. The centroid de-fuzzification technique contributes to enhancing the clarity and precision of the output derived from fuzzy logic systems. The max-min inference approach is used in this instance to identify the resultant output set, which is then used to compute the succeeding output (Su).

Where $\circ$ signifies the operator of composition, hence yielding.

$$\mu_C(\Delta u) = \max_{e.e_c}\left\{\min\left(\mu_{A_i}(e), \mu_{B_i}(e_c), \mu_R(e, e_c, \Delta u)\right)\right\} \quad (21)$$

The output Δu that follows may be shown as

$$\Delta u^* = \frac{\sum_{i=1}^{l} \Delta u_i \mu_c[\Delta u_i]}{\sum_{i=1}^{l} \mu_c[\Delta u_i]} \quad (22)$$

Finally, the value of the fuzzy PI controller's control input u(k) may be written as

International Journal on Recent and Innovation Trends in Computing and Communication
ISSN: 2321-8169 Volume: 11 Issue: 10
Article Received: *25 July 2023* ***Revised:*** *14 September 2023* ***Accepted:*** *28 September 2023*

$$u(k) = u(k-1) + g\Delta u^{*}(k) \qquad (23)$$

where the symbol g stands for the incremental control output gain, which is utilised to quicken the system's reaction time. In this inquiry, the fuzzy subsets "zero (Z)," "positive small (PS)," "positive medium (PM)," "positive big (PB)," and "negative small (NS)" are used. Furthermore, 'negative large (NB)' and 'negative medium (NM)'. For every fuzzy subset, the triangle membership methods are provided for ease of implementation. The purpose of the vertical axis symmetry of these functions is to simplify the implementation process. Furthermore, Tab 1 displays the fuzzy control decision table. The FLC output *u* is able to be described With regard to *e, e_c* and parameters of $a_e, b_e, a_{e_c}, a_{\Delta u}, f_{norm.e}, f_{norm.e_c} and\ g$. Thus, membership function shapes are the main elements affecting control system performance. However, to achieve fuzzy control, the values may be $a_e, b_e, a_{e_c}, a_{\Delta u}, f_{norm.e}, f_{norm.e_c} and\ g$, in order to ensure optimal performance, it is necessary to determine the appropriate normalisation factors and control gain for each membership function. Hence, a performance index is established, accompanied by a proposed algorithm in this document to efficiently search for the optimal values of $a_e, b_e, a_{e_c}, a_{\Delta u}, f_{norm.e}, f_{norm.e_c} and\ g$.

Fuzzy Control Decision table

Weighted absolute errors and change combined together give a performance gauge, which is the inverse of this total:

Table 1 Fuzzy Control Decision Table

Δu \ e	NB	NM	NS	Z	PS	PM	PB
PB	**Z**	PS	PM	*PB*	PB	PB	PB
PM	NS	**Z**	PS	PM	PB	PB	PB
PS	NM	NS	**Z**	PS	PM	PB	PB
Z	NB	NM	NS	**Z**	PS	PM	PB
NS	NB	NB	NM	NS	**Z**	PS	PM
NM	NB	NB	NB	NM	NS	**Z**	PS
NB	NB	NB	NB	NB	NM	NS	**Z**

(e_c →)

Fitness Function: A fuzzy proportional-integral (PI) controller's performance as measured by a set of performance criteria is called its fitness function. This is the case when optimising the gains of the controller. The goal is to design a fitness function that reflects the desired behaviour of the control system and can be used by optimization algorithms to evaluate and improve the controller gains.

$$F = \frac{1}{\sum_{j=1}^{k}\left(w_1\left|e(j)\right| + w_2\left|e_c(j)\right|\right)} \qquad (24)$$

The performance weights $w_1 and\ w_2$ are being discussed here. The larger weight size is associated with equivalent transient reaction, which is of more importance. A higher level of performance is indicated by fitness function F relatively high values.

The suggested method must fulfil all three of the following characteristics in order to be successful in its search for the optimum values of ($a_e, b_e, a_{e_c}, a_{\Delta u}, f_{norm.e}, f_{norm.e_c} and\ g$) that maximise the fitness function :

- The capacity to deal with non-linearity, like fuzzy rules ;
- The ability to tackle large-scale issues;
- Enables fast solution development without stifling at local optimums.

International Journal on Recent and Innovation Trends in Computing and Communication
ISSN: 2321-8169 Volume: 11 Issue: 10
Article Received: *25 July 2023* ***Revised:*** *14 September 2023* ***Accepted:*** *28 September 2023*

RESULT AND DISCUSSION

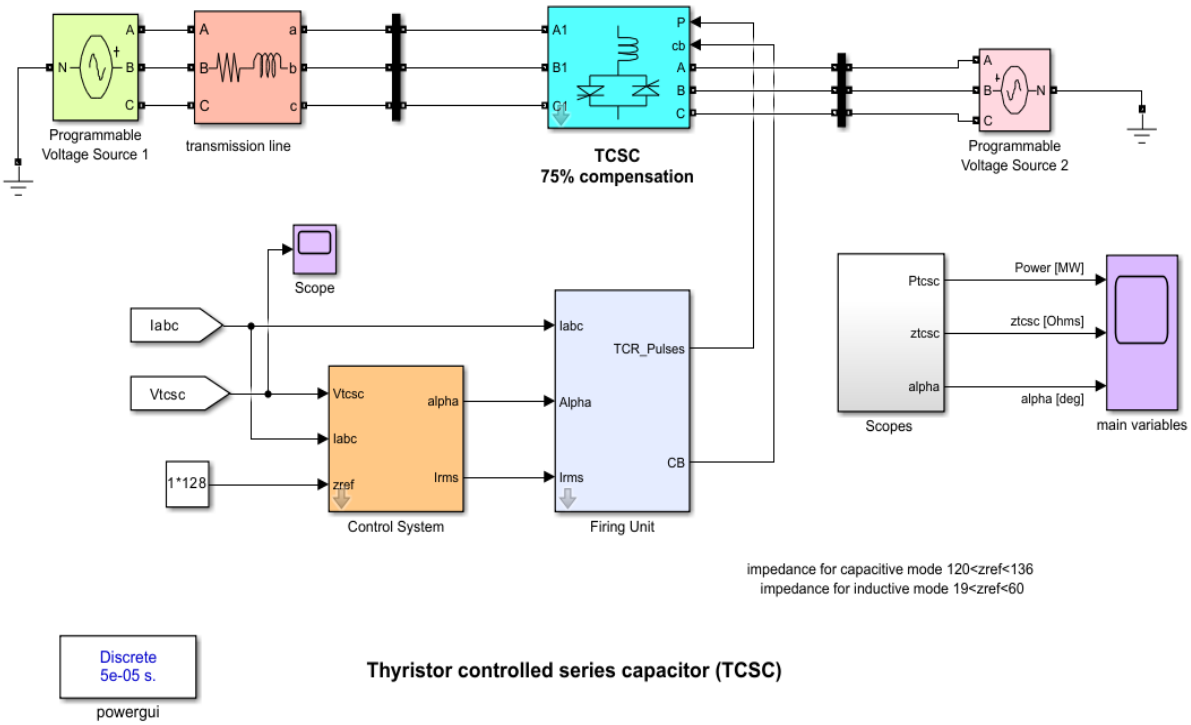

Figure 4 Thyristor controlled series capacitor (TCSC)

Description

To enhance power transfer, a 500kV transmission line is equipped with a TCSC. When the TCSC is disregarded in the first 0.5 seconds of the simulation, power transfer is approximately 110MW without it. Each TCSC phase has a parallel (TCR) & fixed capacitor. At 90 degrees, the nominal correction is 75%, using simply capacitors. The TCSC's natural oscillation frequency is 163 Hz, 2.7 times the fundamental frequency.

Although this type of operation is rarely used in real-world applications, the TCSC may operate in both capacitive & inductive modes. The resonance of this TCSC occurs at a firing range of approximately 58 degrees, consequently operating between 49 and 69 degrees is prohibited. When the line impedance is put into consideration, the total resonance of the system is around 67 degrees Capacitive mode is achieved by firing at 69–90 degrees. Power transfer rises as shot angle decreases because 90 degrees has the lowest impedance. Capacitance mode impedance is 120-136 Ohm. This range corresponds to 490-830 MW power transfer (100%-110% compensation). When contrasted to an uncompensated line which transfers 110 MW of power, TCSC provides for a significant increase in power transfer levels.

The control block dialogue toggle switch switches between inductive, capacitive, & manual operation modes. The inductive mode firing angles are 0-49 degrees, and 0 degrees provides the lowest impedance. The inductive operation mode has 19–60 Ohm impedances or 100–85 MW power transfer. Power transfer along the line is reduced by induction. Same limits apply with a constant firing angle.

TCSC Control

In constant impedance mode, the TCSC determines its impedance using current and voltage feedback. The reference impedance indirectly determines power, but a self-sufficient power control mode is possible.

Each mode uses a separate PI controller. Phase lead compensators are used in capacitive mode. Every controller has an adaptive control loop to improve performance throughout a wide operating range. Impedance differences because system gain variances, which the controller's gain scheduling corrects.

The firing circuit uses three single-phase PLL units to synchronize with line current. Instead of using line voltage for synchronization, line current is utilized as the TCSC voltage may vary significantly while the device is operating.

Simulation

In this simulation we are using matlab version R2023a and the architecture was given below

CASE-I

Absence of TCSC

The TCSC is in capacitance impedance modification mode with a pre-set impedance of 128 Ohm. The circuit breaker is used to avoid the TCSC for the first 0.5 seconds, resulting in a 110 MW power transfer. Power transfer to 610 MW is increased when the TCSC regulates the impedance to 128

International Journal on Recent and Innovation Trends in Computing and Communication
ISSN: 2321-8169 Volume: 11 Issue: 10
Article Received: *25 July 2023* ***Revised:*** *14 September 2023* ***Accepted:*** *28 September 2023*

ohms at 0.5 seconds. To allow for the least amount of switching disruption on the line, the TCSC begins with alpha at 90 degrees.

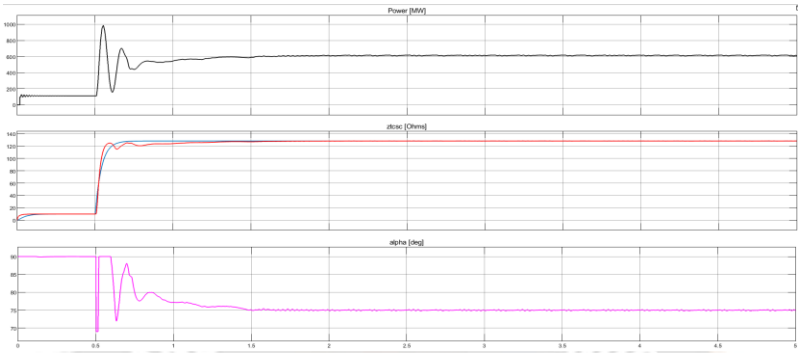

CASE-II

With change reference impendence

A 5% shift in the reference impedance is carried out at 2.5s. According to the response, TCSC permits reference impedance tracking, & the settling time is around 500 ms

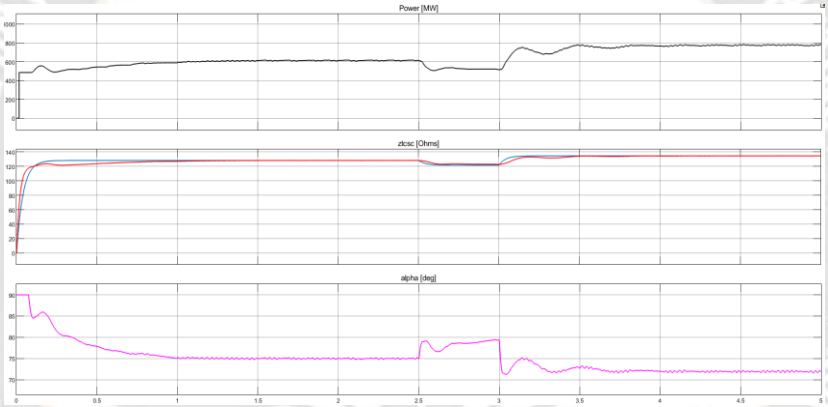

CASE-III

Change in source voltage

The source's voltage is reduced by 4% at 3.3 s, and at 3.8 s, it returns to 1 p.u. It is observed that the TCSC impedance remains constant while the TCSC controller adjusts for these disruptions. The TCSC responds in 200–300 milliseconds.

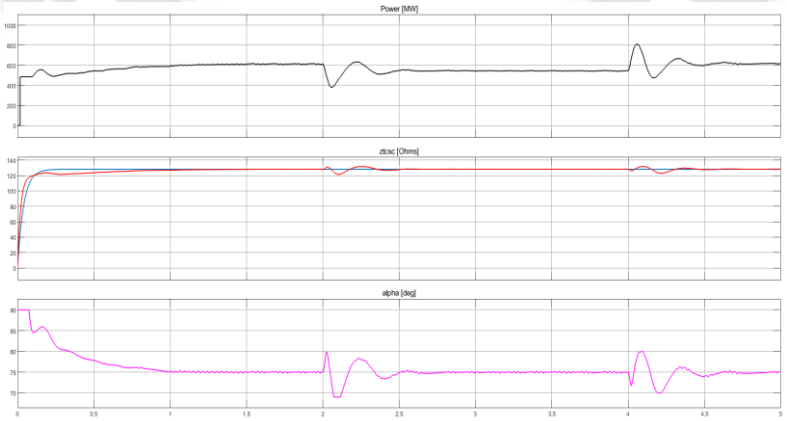

International Journal on Recent and Innovation Trends in Computing and Communication
ISSN: 2321-8169 Volume: 11 Issue: 10
Article Received: *25 July 2023* ***Revised:*** *14 September 2023* ***Accepted:*** *28 September 2023*

Convergence plot

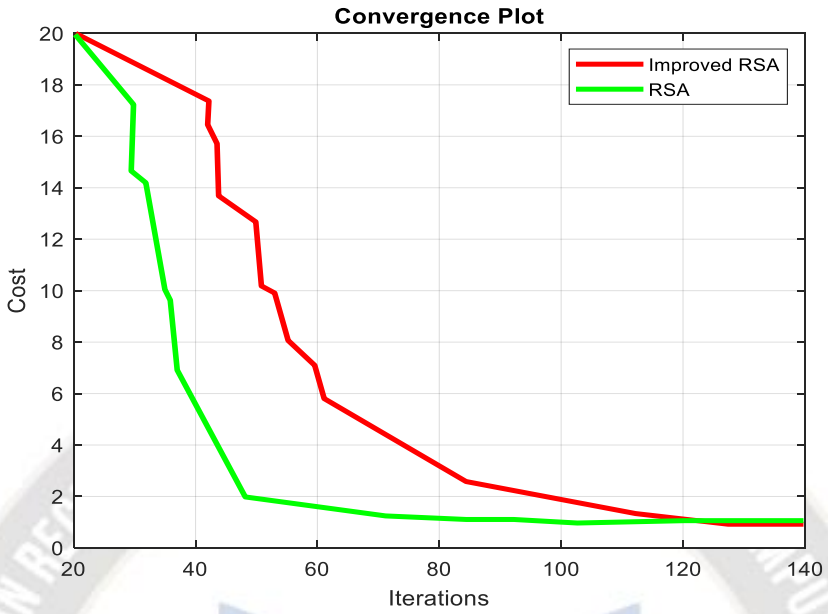

Figure 5 convergence plot

From the above convergence plot we are comparing proposed and other algorithm our proposed algorithm was much better than the RSA.
From the above results they have some parameters from proposed model they are given below

Table 2 parameters

PARAMETERS	CASE-I	CASE-II	CASE-III
Settling Time	18.526	18.52	18.52
Raise Time	82.66	84.642	86.73
overshoot	1.96	0.95	32.966
undershoot	2.38	1.99	40.141

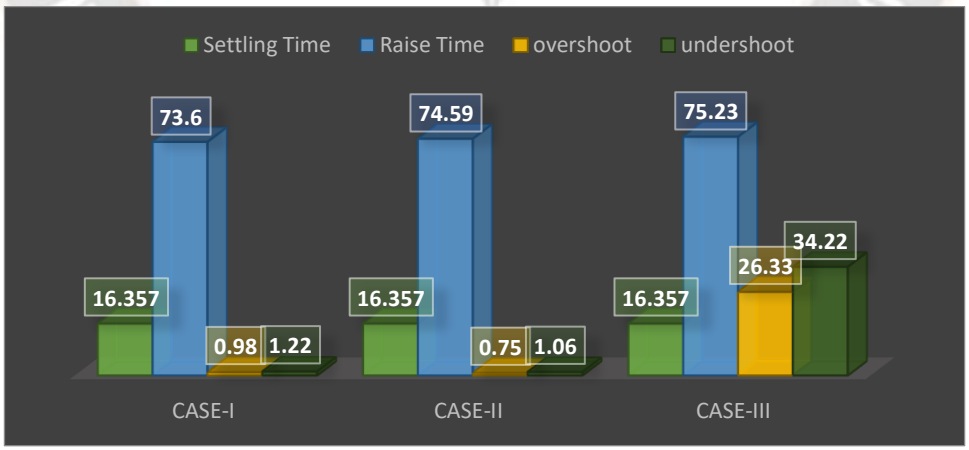

The table.2 and figure presents a comparative analysis of key performance parameters for three distinct cases, labelled as Case-I, Case-II, and Case-III. These cases are associated with the evaluation of power system stability under the influence of Fuzzy-PI cascade controllers. The parameters under scrutiny include Settling Time, Raise Time, Overshoot, and Undershoot. Settling Time, measured in seconds, indicates the time required for the system response to reach and remain within a specified range. In Case-I, Settling Time is reported as 18.526 seconds, while both Case-II and Case-III exhibit the same Settling Time at 18.52 seconds. Raise Time, denoting the time taken for the system response to ascend from a specified lower value to a specified higher value, is documented at 82.66 seconds in Case-I, 84.642 seconds in

International Journal on Recent and Innovation Trends in Computing and Communication
ISSN: 2321-8169 Volume: 11 Issue: 10
Article Received: *25 July 2023* ***Revised:*** *14 September 2023* ***Accepted:*** *28 September 2023*

Case-II, and 86.73 seconds in Case-III. Overshoot, expressed as a percentage, signifies the maximum percentage by which the system response exceeds the steady-state value. Notably, Case-I records an overshoot of 1.96%, while Case-II demonstrates a reduced value of 0.95%. Conversely, Case-III exhibits a significantly higher overshoot at 32.966%. Undershoot, representing the percentage by which the system response falls below the steady-state value, is documented as 2.38% in Case-I, 1.99% in Case-II, and notably elevated at 40.141% in Case-III. This comprehensive analysis provides valuable insights into the dynamic performance of power systems under the influence of Fuzzy-PI controllers in varying scenarios.

With comparison of another algorithm the following results are given below

Table 3 parameters

PARAMETERS	CASE-I	CASE-II	CASE-III
Settling Time	16.357	16.357	16.357
Raise Time	73.6	74.59	75.23
overshoot	0.98	0.75	26.33
undershoot	1.22	1.06	34.22

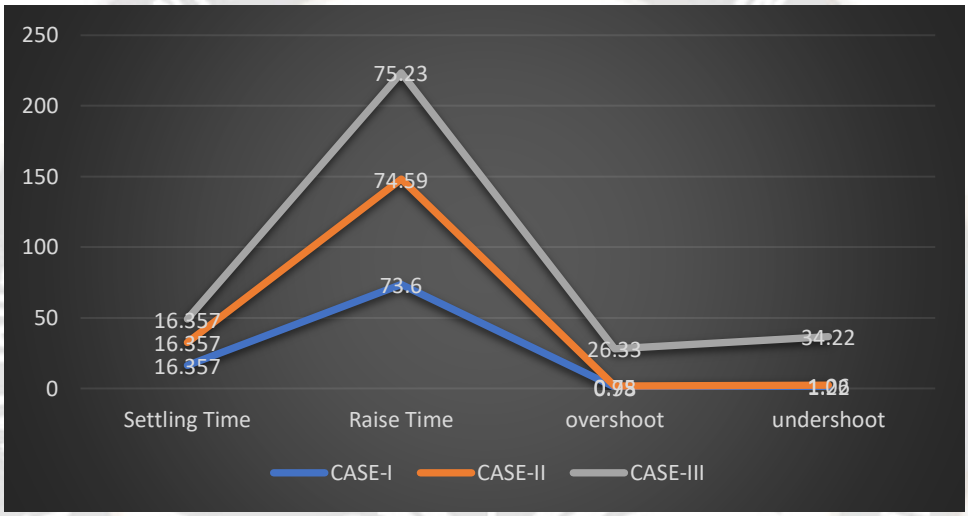

In this comparative analysis, the performance of the proposed Fuzzy-PI cascade controllers, implemented with the improved RSA algorithm, is evaluated against an alternative employing the traditional RSA algorithm across three scenarios: Case-I, Case-II, and Case-III. Both algorithms demonstrate comparable Settling Times, stabilizing at 16.357 seconds, indicating their shared ability to promptly bring the system response within the desired range. Notably, the proposed controllers exhibit a slightly quicker Raise Time in Case-I. However, the most significant distinctions emerge in terms of Overshoot and Undershoot. The proposed Fuzzy-PI controllers consistently outperform the alternative RSA algorithm, showcasing lower Overshoot values in all cases and reduced Undershoot values in Case-I and Case-II. This analysis highlights the efficacy of the proposed Fuzzy-PI controllers with the improved RSA algorithm, underscoring superior performance in mitigating system instabilities and enhancing power system stability compared to the traditional RSA algorithm.

CONCLUSION

In conclusion, the integration of Fuzzy-PI cascade controllers and Thyristor-Controlled Series Compensator (TCSC) represents a promising approach to enhance power system stability. The collaborative application of these advanced control techniques addresses the complex dynamics of power systems, effectively mitigating oscillations and improving overall stability. Through the seamless coordination of the Fuzzy-PI cascade controllers and TCSC, the system exhibits enhanced transient and dynamic responses, minimizing the impact of disturbances. The success of this approach underscores the potential for intelligent control strategies in bolstering power system stability, thereby contributing to the reliability and efficiency of modern power grids. This research lays the foundation for future advancements in power system control methodologies, emphasizing the significance of integrating sophisticated techniques to address the evolving challenges in the field.

REFERENCES

1. S. Sahoo, N. K. Jena, G. Dei, and B. K. Sahu, “Self-adaptive Fuzzy-PI controller for AGC study in deregulated Power System,” *Indones. J. Electr. Eng. Informatics*, vol. 7, no. 4, pp. 650–663, 2019.
2. G. B. Nimmakanti Anil** and *Research, “VOLTAGE STABILITY ENHANCEMENT IN WIND ENERGY

CONVERSION SYSTEM Nimmakanti," vol. 55, no. 02, pp. 31–41, 2023.
3. M. Ranjan and R. Shankar, "A Cascade Fractional Type-II Fuzzy Control Approach for Enhancing Frequency Stability in a Smart Grid System with Diverse Energy Resources," *Iran. J. Sci. Technol. Trans. Electr. Eng.*, vol. 47, no. 4, pp. 1537–1560, 2023.
4. N. M. A. Ibrahim, E. A. El-said, H. E. M. Attia, and B. A. Hemade, "'Enhancing power system stability: an innovative approach using coordination of FOPI controller for PSS and SVC FACTS device with MFO algorithm,'" *Electr. Eng.*, 2023, doi: 10.1007/s00202-023-02051-7.
5. M. Shafiee, M. Sajadinia, A.-A. Zamani, and M. Jafari, "Enhancing the transient stability of interconnected power systems by designing an adaptive fuzzy-based fractional order PI controller," *Energy Reports*, vol. 11, pp. 394–411, 2024.
6. A. H. A. Elkasem, M. Khamies, G. Magdy, I. B. M. Taha, and S. Kamel, "Frequency stability of ac/dc interconnected power systems with wind energy using arithmetic optimization algorithm-based Fuzzy-PI controller," *Sustain.*, vol. 13, no. 21, 2021, doi: 10.3390/su132112095.
7. Z. Farooq, A. Rahman, and S. A. Lone, "Power generation control of restructured hybrid power system with FACTS and energy storage devices using optimal cascaded fractional-order controller," *Optim. Control Appl. Methods*, vol. 43, no. 3, pp. 757–786, 2022.
8. Y. Welhazi, T. Guesmi, I. Ben Jaoued, and H. H. Abdallah, "Power system stability enhancement using FACTS controllers in multimachine power systems," *J. Electr. Syst.*, vol. 10, no. 3, pp. 276–291, 2014.
9. V. Veerasamy *et al.*, "A Hankel Matrix Based Reduced Order Model for Stability Analysis of Hybrid Power System Using PSO-GSA Optimized Cascade PI-PD Controller for Automatic Load Frequency Control," *IEEE Access*, vol. 8, pp. 71422–71446, 2020, doi: 10.1109/ACCESS.2020.2987387.
10. M. Eslami, H. Shareef, and A. Mohamed, "Application of PSS and FACTS devices for intensification of power system stability," *Int. Rev. Electr. Eng.*, vol. 5, no. 2, pp. 552–570, 2010.
11. M. Eslami, H. Shareef, and A. Mohamed, "Application of PSS and FACTS devices for intensification of power system stability," *Int. Rev. Electr. Eng.*, vol. 5, no. 2, pp. 552–570, 2010.
12. M. K. Debnath, T. Jena, and R. K. Mallick, "Optimal design of PD-Fuzzy-PI cascaded controller for automatic generation control," *Cogent Eng.*, vol. 4, no. 1, p. 1416535, 2017.
13. Y. Arya, P. Dahiya, E. Çelik, G. Sharma, H. Gözde, and I. Nasiruddin, "AGC performance amelioration in multi-area interconnected thermal and thermal-hydro-gas power systems using a novel controller," *Eng. Sci. Technol. an Int. J.*, vol. 24, no. 2, pp. 384–396, 2021.
14. M. Almazroi, "IMPROVING POWER SYSTEM STABILITY AND CONTROL IN ALERT AND EMERGENCY STATE BY USING FACTS CONTROL SYSTEM." KING ABDULAZIZ UNIVERSITY, 2023.
15. K. Nithilasaravanan, N. Thakwani, P. Mishra, V. Kumar, and K. P. S. Rana, "Efficient control of integrated power system using self-tuned fractional-order fuzzy PI controller," *Neural Comput. Appl.*, vol. 31, pp. 4137–4155, 2019.
16. S. Gao, Y. Gao, Y. Zhang, and L. Xu, "Multi-strategy adaptive cuckoo search algorithm," *IEEE Access*, vol. 7, pp. 137642–137655, 2019, doi: 10.1109/ACCESS.2019.2916568.
17. B. H. Abed-alguni, "Island-based cuckoo search with highly disruptive polynomial mutation," *Int. J. Artif. Intell.*, vol. 17, no. 1, pp. 57–82, 2019.
18. S. H. H. Madni, M. S. Abd Latiff, S. M. Abdulhamid, and J. Ali, "Hybrid gradient descent cuckoo search (HGDCS) algorithm for resource scheduling in IaaS cloud computing environment," *Cluster Comput.*, vol. 22, no. 1, pp. 301–334, 2019, doi: 10.1007/s10586-018-2856-x.